Journal of Biomechanics 93 (2019) 11–17

Contents lists available at ScienceDirect

Journal of Biomechanics

journal homepage: www.elsevier.com/locate/jbiomech
www.JBiomech.com

Central screw use delays implant dislodgement in osteopenic bone but not synthetic surrogates: A comparison of reverse total shoulder models

Michael W. Hast [a,*], Matthew Chin [a], Elaine C. Schmidt [a], Andrew F. Kuntz [b]

[a] Biedermann Lab for Orthopaedic Research, Department of Orthopaedic Surgery, The University of Pennsylvania, Philadelphia, PA 19104, USA
[b] Shoulder and Elbow Service, University of Pennsylvania, Department of Orthopaedic Surgery, Philadelphia, PA 19104, USA

ARTICLE INFO

Article history:
Accepted 3 June 2019

Keywords:
Reverse total shoulder
Fixation
Micromotion
Catastrophic failure
Osteopenia
Osteoporosis

ABSTRACT

Adequate glenoid baseplate fixation in reverse total shoulder arthroplasty (rTSA) is important to achieve, but may prove challenging in the context of glenoid bone loss or osteopenia. Current rTSA testing standards rely upon synthetic bone surrogates, but it is unclear if these models accurately recapitulate the mechanics of osteoporotic bone. Additionally, it also unknown if the use of a central screw effectively provides resistance to micromotion in the milieu of poor quality bone. The purpose of this experiment was to create a novel cyclic load test protocol that elicited clinically relevant failures, so that comparisons of relative motion between baseplates and bones could be made with: (1) synthetic bones and poor quality cadaveric bones, and (2) the use or omission of a central screw. rTSA components were implanted into cadaveric and synthetic bones with and without a central screw. To model a range of loads that may be experienced during abduction, increasing cyclic loads were applied to shoulder joints in 30° of humeral abduction. Cycles and loads prior to permanent deformation exceeding 150 μm, 1 mm, and joint failure were determined using measurements from the test frame and from 3-D motion analysis. Synthetic bones demonstrated significantly more resistance to micromotion in comparison to cadaveric bones. Use of the central screw improved resistance to dislodgement, which was only observed in the cadaveric specimens. This study highlights the need for biomechanical testing with cadaveric specimens, especially when assessing osteopenic or osteoporotic populations.

1. Introduction

Reverse total shoulder arthroplasty (rTSA) has become a widely accepted solution for a variety of pathologies. Indications include rotator cuff tear arthropathy, failed shoulder arthroplasty, comminuted proximal humerus fractures in the elderly, and other shoulder impairments that are not reparable with traditional shoulder arthroplasty (Chebli et al., 2008; Cheung et al., 2011; Frankle et al., 2005; Garrigues et al., 2012; Gerber et al., 2009; Guery et al., 2006; Wall et al., 2007). Despite the popularity of rTSA, a broad meta-analysis of this surgery indicates there is a high complication rate (24%) associated with the procedure (Zumstein et al., 2011). A series of clinical outcome studies on the general population have reported glenoid loosening rates between 0 and 12% (Alentorn-Geli et al., 2014; Boileau, 2016; Frankle et al., 2005; Guery et al., 2006; Sirveaux et al., 2004; Stechel et al., 2010; Werner et al., 2005; Zumstein et al., 2011), and scapular fractures ranging between 0.9% and 7.2% (Crosby et al., 2011; Hattrup, 2010; Otto et al., 2013). It is known that these complications are exacerbated in the elderly population due to a limited amount of quality bone stock available for fixation (Cheung et al., 2011; Codsi and Iannotti, 2008; Klein et al., 2010; Lenarz et al., 2011; Otto et al., 2013).

Previously published biomechanical studies have sought to characterize and make improvements in rTSA baseplate fixation. Changes in overall design, baseplate position, and glenosphere lateral offset have been shown to directly impact micromotion and long-term baseplate stability (Elwell et al., 2017; Gutiérrez et al., 2007; Harman et al., 2005; Irlenbusch and Kohut, 2015; Nyffeler et al., 2005; Parsons et al., 2009; Stephens et al., 2015). Other studies have investigated the anatomy of the scapula and identified regions that maximize screw purchase and fixation strength (Codsi and Iannotti, 2008; DiStefano et al., 2011; Humphrey et al., 2008; Stephens et al., 2015). Experiments have also investigated the role of individual screws in baseplate fixation. Examples include peripheral screws (Chebli et al., 2008; Elwell et al., 2017; James et al., 2013; Yang et al., 2013), posterior screws (Hoenig

* Corresponding author at: Biedermann Lab for Orthopaedic Research, 3737 Market Street, 10th Floor Suite 1050, The University of Pennsylvania, Philadelphia, PA 19104, USA.
E-mail address: hast@pennmedicine.upenn.edu (M.W. Hast).

https://doi.org/10.1016/j.jbiomech.2019.06.004
0021-9290/

et al., 2010), the central screw (Königshausen et al., 2015), and locking versus non-locking screws (Chebli et al., 2008; Humphrey et al., 2008; Stephens et al., 2015). Interestingly, none of these studies were performed with osteopenic or osteoporotic bone, which is a common comorbidity associated with this patient population.

In general, there are three methods that have been used to test glenoid baseplate fixation in rTSA implants. First, the humerus can be moved inferiorly and superiorly relative to the scapula under load control (Harman et al., 2005; Irlenbusch and Kohut, 2015) (Fig. 1A). This model recreates implant loosening with a rocking horse mechanism, but the loading parameters are not necessarily representative of those experienced during activities of daily living, especially for patients whom have a deficient rotator cuff. As a second option, the shoulder joint can be set at a fixed abduction angle and external loads can be imparted along the long axis of the humerus (Fig. 1B) (Codsi and Iannotti, 2008; Gutiérrez et al., 2007; Martin et al., 2017). This type of test is easy to perform with standard uniaxial testing machines, but only provides simulations of a limited range of motion. Third, the shoulder can be moved through a dynamic range of joint angles while external loads are applied (Fig. 1C) (Chebli et al., 2008; Formaini et al., 2015; Hoenig et al., 2010; Roche et al., 2013a, 2013b; Stroud et al., 2013). This protocol represents the preferred ASTM standard for testing rTSA implants (ASTM F2028-17, 2017). However, the testing equipment required to perform this protocol is not as commonplace as uniaxial universal test frames, and thus may not be readily performed in many biomechanics labs.

Synthetic bone models have become a standard for biomechanical studies involving rTSA components (Chebli et al., 2008; Codsi and Iannotti, 2008; Formaini et al., 2015; Gutiérrez et al., 2007; Harman et al., 2005; Hoenig et al., 2010; Irlenbusch and Kohut, 2015; Königshausen et al., 2015; Martin et al., 2017). The rationale for the use of synthetic bones is threefold: (1) they effectively reduce the variability in experimental measures (Elfar et al., 2014), (2) they are less costly to procure, and (3) they are not biohazardous. However, there still remains a need to perform experiments on human tissues, especially cadaveric bone of poor quality. Currently, there are no in vitro studies that investigate rTSA baseplate fixation in the presence of osteopenic or osteoporotic bone.

The purpose of this experiment was to create a novel cyclic load test protocol that elicited clinically relevant failures, so that two main goals could be accomplished. First, to compare relative motion between rTSA glenoid baseplates with synthetic bones and poor quality cadaveric bones. It was hypothesized that synthetic bones would demonstrate significantly increased resistance to micromotion and implant dislodgement. The second goal was to characterize the role of the central screw in baseplate fixation for a specific implant. It was hypothesized that the use of a central screw would provide additional resistance to micromotion and the implant would sustain a higher number of cyclic loads prior to dislodgement.

2. Materials and methods

The cadaveric portion of this study was performed with eight matched pairs of fresh-frozen scapulae (3 male, 5 female; average age: 80.6 years, range: 73–88 years). DEXA scans were performed prior to the acquisition of specimens to confirm osteopenia (Supplemental Table 1). As a synthetic surrogate for osteoporotic bones, closed cell polyurethane bone blocks were used (15 lb per cubic foot Sawbones, Pacific Research Laboratories, Vashon Island, WA; n = 3 per group). Sample sizes were determined with a power analysis based on results from a previous study that tested rTSA glenoid baseplate fixation to failure (Chebli et al., 2008) (see Appendix A for more details).

2.1. Specimen preparation

Intact upper extremity specimens were thawed for 24 h prior to the day of gross dissection. Scapulae were disarticulated from the shoulder girdle and skeletonized. Prepared specimens were subsequently refrozen at −20 °C. On the day of surgery, specimens were defrosted at room temperature for approximately 2 h and baseplate implantation was performed by a single fellowship-trained orthopaedic surgeon (AFK), using the Titan Reverse Total Shoulder System (Integra Life Sciences, Plainsboro, NJ). The left and right scapulae of the matched pairs were randomly assigned to either cadaveric central screw positive (C+) or cadaveric central screw negative (C−) groups (Fig. 2). C+ and C− specimens underwent normal baseplate implantation per manufacturer guidelines which included the use or omission of a central screw (5.5 mm diameter, 20 mm long; Appendix B). Once implantation was complete, the scapulae were osteotomized and potted in polycarbonate cylinders filled with polymethylmethacrylate (PMMA) (OrthoJet, Lang Dental, Wheeling, IL). Pots were filled up to 1 cm medial from the nadir of concavity of the glenoid. Prepared specimens were frozen at −20 °C until the day of biomechanical testing.

Synthetic bone blocks were cut into cylinders (diameter: 10 cm, height: 3.75 cm) and subsequently cemented into polycarbonate tubes with PMMA. The procedures described above were used for implantation to create synthetic with central screw (S+) and synthetic without central screw (S−) groups (Fig. 2).

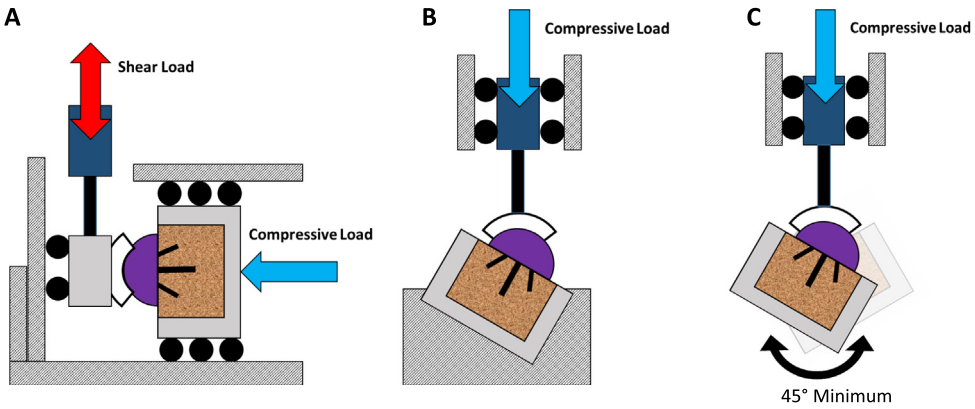

Fig. 1. Schematic diagrams showing test protocols used to apply compressive forces and shear displacements (A), isolated compressive forces (B), and compressive forces with dynamic rotation of the joint (C).

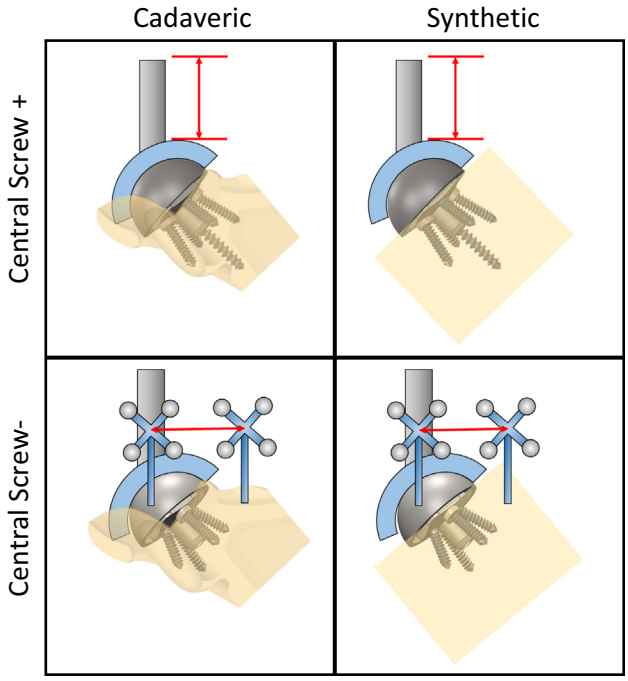

Fig. 2. Schematic drawings of the variables of interest tested in the study. Cadaveric and synthetic bone testing is represented in the vertical columns, while the use and omission of the central screw is represented in the horizontal rows. Representations of the actuator-based and 3-D motion tracking measures are also shown (red arrows). (For interpretation of the references to colour in this figure legend, the reader is referred to the web version of this article.)

2.2. Biomechanical testing

Implanted specimens were defrosted to room temperature on the day of biomechanical testing. Once thawed, marker clusters were rigidly affixed to custom 3-D printed jigs, which were either screwed into to the scapula/bone block or glued to the glenosphere, for the purposes of 3-D motion capture (see Appendix C). A 6-camera motion capture system (Optitrack Motive, Natural Point, Corvallis, OR) was calibrated to a 0.2 mm threshold of accuracy. 5 s recordings of marker trajectories were made every 100 s throughout the course of cyclic testing (described below). Custom-made software (MATLAB R2017b, Natick, MA) was developed to calculate the 3-D relative displacement between the scapula and glenosphere using validated 3-D motion tracking techniques (Winter, 1990).

The following methods were used to create the testing jig (Fig. 3). The humeral stem was potted in a polycarbonate tube with a low melting point alloy (Cerralow 117, McMaster-Carr, Robbinsville, NJ) and attached to the vertical actuator of the test frame (Electroforce 3330, TA Instruments, New Castle, DE, 3 kN load cell, 1 nm displacement resolution (TA Instruments ElectroForce 3330 Data Sheet, 2015)). An adjustable-angle vise was used to hold the potted scapulae at 30° abduction relative to the humeral stem. This created a contact force vector with a direction similar to vectors measured with telemetered implants during 90° abduction (mean 31.7° superomedially) (Bergmann et al., 2011; Westerhoff et al., 2009). The vise was securely attached to the floor of a tank. A 37 °C circulating water bath was used to test cadaveric specimens, while synthetic bone specimens were tested in 23 °C air. A stainless steel rail was attached to the bottom surface of the tank, which slid on a linear bearing affixed to the frame. Compressive horizontal loads of 100 N were applied to the glenohumeral joint, which is a reasonable approximation of joint loads on the shoulder during quiet standing (Nikooyan et al., 2010). These forces were imparted onto the sliding tank with a pneumatic cylinder, and were recorded with an Arduino-powered load cell (Technology Co., Xian, China).

Increasing cyclic loads were imparted onto the specimens with the vertical actuator using a 1 Hz sinusoidal waveform, which steadily increased the maximum loads at a rate of 0.2 N/cycle. The first waveform had a minimum compressive load of 100 N and a peak of 150 N (180 N resultant load). This represents modest glenohumeral joint loads during various activities of daily living (Bergmann et al., 2011; Nikooyan et al., 2010; Westerhoff et al., 2009). The protocol was designed to have 13,500 cycles (which exceeds the 10,000 recommended by the ASTM standard), such that the final waveform had a maximum load of 2850 N (95% saturation of our 3 kN load cell). Specimens were cycled until dislodgement of the baseplate or joint disarticulation, which caused the test frame to stop instantly. Micromotion was measured by quantifying permanent creep between the bone-baseplate interface in two manners (Fig. 2): (1) measurements from the vertical actuator displacement, and (2) calculating 3-D Euclidean distances between the bones and implant, based on motion capture cluster trajectories. Threshold values of 150 μm, and 1 mm were used, and the rationale for these choices will be delineated later in the Section 4.

2.3. Statistical analysis

The number of cycles survived before micromotion thresholds and implant dislodgement or joint disarticulation were compared using SigmaStat 4.0 (Systat, San Jose, CA). Data sets were first checked for normality and equal variance with Shapiro-Wilk and Brown-Forsythe tests, respectively. If they passed these tests, one-way ANOVAs were performed and the Holm-Sidak method was employed to make relevant pairwise comparisons between groups. If the data set failed the normality test, a Kruskall-Wallis one-way ANOVA based on ranks was performed and Dunn's method was used to make pairwise comparisons between groups.

3. Results

The model successfully recreated realistic dislodgement events in cadaveric specimens (Bohsali et al., 2006) (Fig. 4), but synthetic bone trials resulted in joint disarticulation. This was caused by impingement between the rim of the polyethylene cup and the synthetic bone block (Appendix D). Comparisons of cycles to joint failure (cadaveric: dislodgement, synthetic: dislocation) indicated that S− survived an average of 72.4% more cycles than the C− ($p = 0.004$), while S+ survived an average of 69.7% more cycles than C+ ($p = 0.077$) (Fig. 5, Supplemental Table 2). Due to differences in failure criteria, an additional 1-tailed paired *t*-test was used to compare the C+ and C− matched pairs only. Based on this analysis, the use of a central screw significantly increased the number of cycles survived before dislodgement by 23.2% ($p = 0.026$). Loads associated with final cycles can be found in Supplemental Tables 2–4.

When using actuator displacement as a micromotion measurement tool, several changes in behavior were observed across test materials. (Fig. 6A. Supplementary Tables 3A&B and 4A&B). For the 1 mm measures, C+ survived an average of 37.8% fewer cycles than S+ ($p = 0.039$) and on average C− survived 45.0% fewer cycles than S− ($p = 0.019$). For smaller permanent displacements of 150 μm, there were no significant differences between test mediums. Use of the central screw resulted in no significant differences between groups at both 1 mm and 150 μm.

Comparisons of micromotions with motion capture techniques did not provide the same amount of resolution as actuator-based

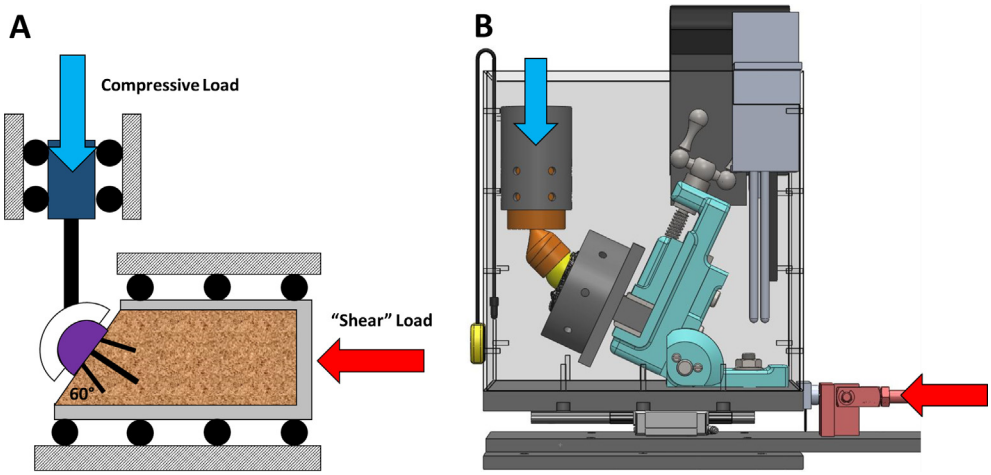

Fig. 3. Schematic (A) and computer-aided drawing (B) of the testing apparatus. Water was circulated with an aquarium filter (black). Bath temperature was controlled with a submersible heater (gray) and monitored with a thermocouple (yellow). Compressive vertical loads (blue arrow) were applied by the actuator through the humeral stem (orange) onto the glenosphere (yellow). The entire apparatus slid on a linear bearing, located underneath the tank. This permitted a horizontal load (red arrow) to be applied with the piston of a pneumatic cylinder (red). (For interpretation of the references to colour in this figure legend, the reader is referred to the web version of this article.)

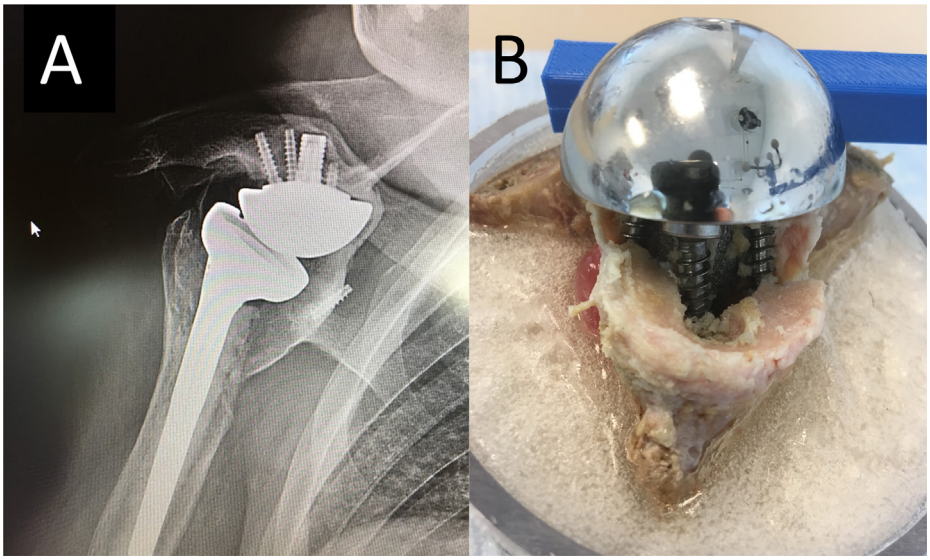

Fig. 4. (A) Radiograph of a failed Integra Titan rTSA glenoid baseplate, where the implant has torn out of the glenoid and is now lodged in the scapular spine. (B) Photograph depicting catastrophic failure of baseplate fixation in the cadaveric model.

measurements (Fig. 6B, Supplementary Table 4C&D). For the 1 mm measures, C+ survived an average of 63.0% fewer cycles than S+ but, due to large standard deviations in the cadaveric measurements, these results were not statistically significant ($p = 0.312$). Similarly, C− survived an average of 53.2% fewer cycles than S-, but results were not statistically significant ($p = 0.981$). Due to the limitations in resolution of the motion analysis setup (~200 μm), no reliable data could be collected for 150 μm displacements.

4. Discussion

This study was based upon developing a mechanical testing paradigm that reliably recapitulated clinically relevant rTSA failure mechanisms in the presence of osteopenic bone. It contains three notable departures from the existing ASTM standards (ASTM F2028-17, 2017). First, this study used increasing cyclic loads, whereas the ASTM standard simulates repeated compressive loads of 750 N. The use of increasing cyclic loads is an important aspect of this technique. It allows for the quantification of maximum forces that can be withstood during early rehabilitation. This is especially pertinent, because early return to activity can improve overall clinical success rates (Boudreau et al., 2007; Wall et al., 2007), but this must be weighed against the risk of implant loosening. Second, similar to previous studies (Codsi and Iannotti, 2008; Gutiérrez et al., 2007; Martin et al., 2017), this experiment applies a static superomedially oriented joint contact vector. We think that this is a reasonable approximation of the mean vector direction throughout 90° abduction motions (Bergmann et al., 2011; Westerhoff et al., 2009). Third, because water acts both as a lubricant and a temperature controller, the ASTM standard for *anatomic* shoulder implants calls for testing to take place in a 37 °C water bath (ASTM F2028-17, 2017). Interestingly, the standard for *reverse* total shoulder components calls for synthetic specimens to be tested in room temperature air. To highlight differences between existing standards and the current experiment, the cadaveric spec-

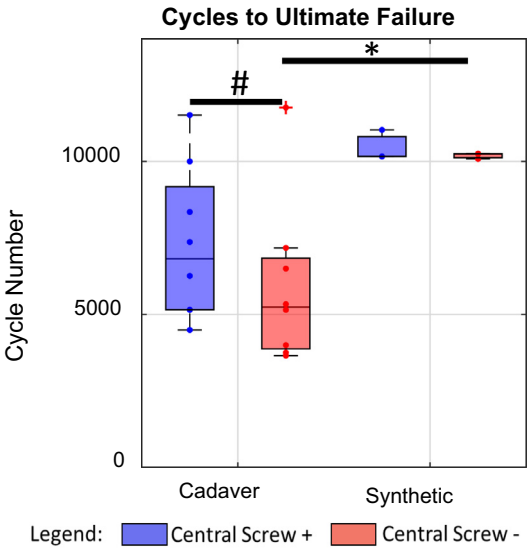

Fig. 5. Box and whisker plot showing cycles prior to dislodgement or disarticulation for the cadaveric and synthetic bone groups, respectively. Significant increases in cycles to failure and were found between the C– and C+, as indicated by * ($p = 0.004$). A one-tailed, paired *t*-test indicated significant differences between the C+ and C– groups, as indicated by # ($p = 0.026$).

imens were tested in 37 °C water while the synthetic blocks were tested in room temperature air. Future studies will be performed to identify the differences between heated bath and room temperature tests with synthetic bones.

The methods described in this paper have associated pros and cons. Advantages of actuator displacement measures include high resolution (~1 nm), continuous data collection, and a low signal-noise ratio. However, actuator displacement only measures the one-dimensional creep of the entire testing jig. The use of 3-D motion capture eliminates some of these shortcomings, as it provides a 3-D measure of the displacement between the glenosphere-baseplate construct and the bone. Aside from obvious problems associated with poor resolution, 3-D motions were only collected every 100 cycles, and the marker clusters attached to soft bone had the potential to shift during testing. This ultimately introduced large standard deviations into the dataset (Fig. 6). Finally, the use of cadaveric specimens provides more realistic simulations of implant fixation, but such specimens come with a high financial burden and inherent variability.

To our knowledge, this is the first study that has assessed glenoid baseplate fixation with both synthetic bones and confirmed osteopenic cadavers. Results partially confirmed our hypothesis that osteopenic specimens were less robust than synthetic bones, as this behavior only became apparent in 1 mm and dislodgement analyses (Figs. 5 and 6). Previous studies have relied upon a 150 μm resultant relative movement threshold as a gold standard (Codsi and Iannotti, 2008; Gutiérrez et al., 2007; Irlenbusch and Kohut, 2015; James et al., 2013; Martin et al., 2017). This generally accepted displacement threshold is known to promote osseous integration and long-term fixation in bone (ASTM F2028-17, 2017; Cameron et al., 1973; Jasty et al., 1997; Pilliar et al., 1986). Interestingly, the loads associated with 1 mm permanent displacement for C+ and C– were 754 ± 742 N and 778 ± 725 N, respectively. If the ASTM standards (750 N) were followed directly with our cadaveric specimens, it is presumed that approximately 1 mm of implant displacement would have occurred on the first cycle for most specimens.

Some discrepancies between synthetic and cadaveric results may attributed to differences in geometry. The synthetic bone blocks were able to distribute stresses from the screws uniformly, whereas the strength of the cadaveric specimens was limited by the small cross-sectional area of the neck of the glenoid. The cadaveric specimens were potted into PMMA up to 1 cm from the nadir of concavity of the glenoid, which is different from previous studies

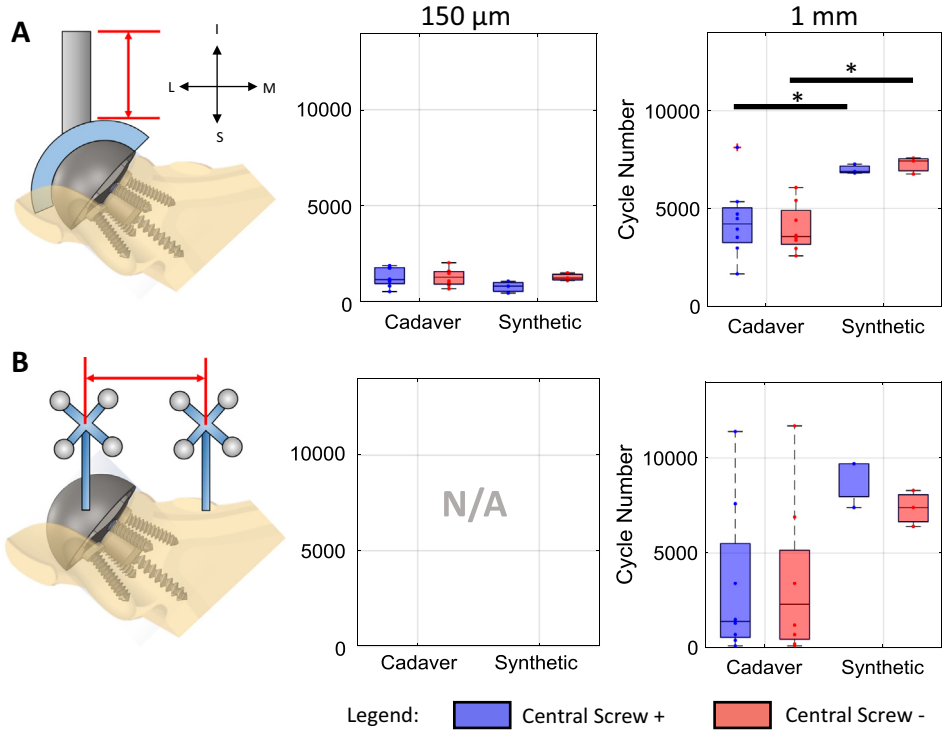

Fig. 6. Box and whisker plots showing cycles to 150 and 1000 μm thresholds, as measured by (A) actuator displacement, and (B) 3-D motion capture. Significant differences were observed in the 1000 μm threshold between test mediums when measured by actuator displacement, as indicated by * ($p < 0.05$).

that buried the majority of the bone in cement (Hoenig et al., 2010; James et al., 2013). This technique ensured that stresses were concentrated at the glenoid neck, and resulted in clinically relevant failure mechanisms (Fig. 4). However, these techniques still prevented scapular spine fractures, which are a more common failure mode seen clinically (Crosby et al., 2011; Hattrup, 2010; Otto et al., 2013). It is currently unclear if anatomically shaped synthetic bones would perform similar to cadaveric bones this milieu, or how different potting methods may result in new fracture patterns. These questions may be pursued in future studies.

The second goal of this study was to investigate the role of the central screw with regard to baseplate fixation. In accordance with our hypothesis, the absence of the central screw significantly reduced the cyclic loads before implant dislodgement in cadavers. This result may be due to the additional depth that is added to the implant construct by the central screw, which aids in resisting moments applied by external loads (Königshausen et al., 2015). Although the premise and loading protocol of this study is unique, the results are similar to the findings of previous experiments, where significant reductions in ultimate failure loads were found when a single screw was removed from any of the peripheral fixation points (Chebli et al., 2008) or different peg lengths were used (Königshausen et al., 2015). Finally, the results showed use or omission of the central screw resulted in no differences in micromotion. This behavior was observed in a baseplate fixation study, where 4 peripheral screws versus 2 peripheral screws exhibited no significant differences in micromotion (James et al., 2013).

This experiment has several overall limitations. First, the use of a cadaveric model only assesses initial fixation, and does not account for osseous integration between the baseplate and glenoid bone. Second, the use of optical 3-D marker tracking precluded our ability to measure 3-D displacements in the range of 150 μm. Future iterations may utilize submersible LVDTs (James et al., 2013; Martin et al., 2017), or employ a laser extensometer. Third, only one shoulder joint angle was modeled in this study. In the future, the vise may be discretely adjusted to investigate a larger range of contact vectors (Gutiérrez et al., 2007), which would also elucidate the effect of shear forces on micromotion (Chae et al., 2016, 2014). Finally, only one implant design was used in this study, so the findings presented may not directly transfer to other implant designs.

4.1. Clinical perspective

Results of the current study represent the first portion of a larger body of work that will be performed in the future. Although dislodgement of the entire glenoid construct (often coupled with fracture of the glenoid vault) is relatively rare (Bohsali et al., 2006) the consequences can be devastating. Prior studies have demonstrated decreased bone ingrowth and formation of a fibrous tissue when implants are displaced between 150 and 500 μm (Cameron et al., 1973; Goodman and Aspenberg, 1992; Jasty et al., 1997; Pilliar et al., 1986). However, the 1 mm measurement is also important, as this represents the approximate displacement that can be observed radiographically in post-operative clinical follow-up. The implant stability required to allow for bone ingrowth may be difficult to achieve in osteopenic bone. Therefore, the role of the central screw may be even more critical to prevent eventual catastrophic failure if bone ingrowth is not achieved.

5. Conclusion

This study introduced a novel rTSA implant testing paradigm that demonstrated the differences between synthetic bones to cadaveric bones with confirmed osteopenia or osteoporosis. The study also examined the role of the central screw with respect to micromotion and implant dislodgement, and found that use of the screw improved the number of cycles that could be survived before dislodgement, but did not affect micromotion. Optimizing screw fixation in poor quality bone is an important clinical issue that requires further research, especially as osteoporosis becomes more commonplace with an aging population.

Acknowledgements

This study was funded by Integra LifeSciences.

Declaration of Competing Interest

Research support from this project was provided by Integra LifeSciences. We can collectively confirm that this relationship did not inappropriately influence our work on this project. For clarity, below is a list of current disclosures for all authors:

MWH: This author, their immediate family, and any research foundation with which they are affiliated did not receive any financial payments or other benefits from any commercial entity related to the subject of this article. For clarity, below is a list of current disclosures for Dr. Hast.

- DePuy Synthes: Research support.
- Integra: Research support.
- Zimmer Biomet: Research support.

MC: This author, their immediate family, and any research foundation with which they are affiliated did not receive any financial payments or other benefits from any commercial entity related to the subject of this article.

ECS: This author, their immediate family, and any research foundation with which they are affiliated did not receive any financial payments or other benefits from any commercial entity related to the subject of this article.

AFK: This author, their immediate family, and any research foundation with which they are affiliated did not receive any financial payments or other benefits from any commercial entity related to the subject of this article. For clarity, below is a list of current disclosures for Dr. Kuntz.

- American Board of Orthopaedic Surgery, Inc.: Board or committee member.
- Integra Life Sciences: Research support.
- Orthofix, Inc.: Research support.
- Orthopaedic Research Society: Board or committee member

Appendix A. Supplementary material

Supplementary data to this article can be found online at https://doi.org/10.1016/j.jbiomech.2019.06.004.

References

Alentorn-Geli, E., Guirro, P., Santana, F., Torrens, C., 2014. Treatment of fracture sequelae of the proximal humerus: comparison of hemiarthroplasty and reverse total shoulder arthroplasty. Arch. Orthop. Trauma Surg. 134, 1545–1550. https://doi.org/10.1007/s00402-014-2074-9.

ASTM F2028-17 Standard Test Methods for Dynamic Evaluation of Glenoid Loosening or Disassociation, 2017. ASTM Int. https://doi.org/10.1520/F2028-17.

Bergmann, G., Graichen, F., Bender, A., Rohlmann, A., Halder, A., Beier, A., Westerhoff, P., 2011. In vivo gleno-humeral joint loads during forward flexion and abduction. J. Biomech. 44, 1543–1552. https://doi.org/10.1016/j.jbiomech.2011.02.142.

Bohsali, K.I., Wirth, M.A., Rockwood, C.A., 2006. Complications of total shoulder arthroplasty. J. Bone Joint Surg. Am. 88, 2279–2292. https://doi.org/10.2106/JBJS.F.00125.

Boileau, P., 2016. Complications and revision of reverse total shoulder arthroplasty. Orthop. Traumatol. Surg. Res., 2015 Instructional Course Lectures (SoFCOT) 102, S33–S43. https://doi.org/10.1016/j.otsr.2015.06.031.
Boudreau, S., Boudreau, E.D., Higgins, L.D., Wilcox III, R.B., 2007. Rehabilitation following reverse total shoulder arthroplasty. J. Orthop. Sports Phys. Ther. 37, 734–743.
Cameron, H.U., Pilliar, R.M., Macnab, I., 1973. The effect of movement on the bonding of porous metal to bone. J. Biomed. Mater. Res. 7, 301–311. https://doi.org/10.1002/jbm.820070404.
Chae, S.-W., Kim, S.-Y., Lee, H., Yon, J.-R., Lee, J., Han, S.-H., 2014. Effect of baseplate size on primary glenoid stability and impingement-free range of motion in reverse shoulder arthroplasty. BMC Musculoskelet. Disord. 15, 417. https://doi.org/10.1186/1471-2474-15-417.
Chae, S.-W., Lee, H., Kim, S.M., Lee, J., Han, S.-H., Kim, S.-Y., 2016. Primary stability of inferior tilt fixation of the glenoid component in reverse total shoulder arthroplasty: a finite element study. J. Orthop. Res. Off. Publ. Orthop. Res. Soc. 34, 1061–1068. https://doi.org/10.1002/jor.23115.
Chebli, C., Huber, P., Watling, J., Bertelsen, A., Bicknell, R.T., Matsen, F., 2008. Factors affecting fixation of the glenoid component of a reverse total shoulder prothesis. J. Shoulder Elbow Surg. 17, 323–327.
Cheung, E., Willis, M., Walker, M., Clark, R., Frankle, M.A., 2011. Complications in reverse total shoulder arthroplasty. J. Am. Acad. Orthop. Surg. 19, 439–449.
Codsi, M.J., Iannotti, J.P., 2008. The effect of screw position on the initial fixation of a reverse total shoulder prosthesis in a glenoid with a cavitary bone defect. J. Shoulder Elbow Surg. 17, 479–486. https://doi.org/10.1016/j.jse.2007.09.002.
Crosby, L.A., Hamilton, A., Twiss, T., 2011. Scapula fractures after reverse total shoulder arthroplasty: classification and treatment. Clin. Orthop. Relat. Res. 469, 2544. https://doi.org/10.1007/s11999-011-1881-3.
DiStefano, J.G., Park, A.Y., Nguyen, T.-Q.D., Diederichs, G., Buckley, J.M., Montgomery, W.H., 2011. Optimal screw placement for base plate fixation in reverse total shoulder arthroplasty. J. Shoulder Elbow Surg. 20, 467–476. https://doi.org/10.1016/j.jse.2010.06.001.
Elfar, J., Stanbury, S., Menorca, R.M.G., Reed, J.D., 2014. Composite bone models in orthopaedic surgery research and education. J. Am. Acad. Orthop. Surg. 22, 111–120. https://doi.org/10.5435/JAAOS-22-02-111.
Elwell, J., Choi, J., Willing, R., 2017. Quantifying the competing relationship between adduction range of motion and baseplate micromotion with lateralization of reverse total shoulder arthroplasty. J. Biomech. 52, 24–30. https://doi.org/10.1016/j.jbiomech.2016.11.053.
Formaini, N.T., Everding, N.G., Levy, J.C., Santoni, B.G., Nayak, A.N., Wilson, C., Cabezas, A.F., 2015. The effect of glenoid bone loss on reverse shoulder arthroplasty baseplate fixation. J. Shoulder Elbow Surg. 24, e312–e319.
Frankle, M., Siegal, S., Pupello, D., Saleem, A., Mighell, M., Vasey, M., 2005. The Reverse Shoulder Prosthesis for glenohumeral arthritis associated with severe rotator cuff deficiency. A minimum two-year follow-up study of sixty patients. J. Bone Joint Surg. Am. 87, 1697–1705. https://doi.org/10.2106/JBJS.D.02813.
Garrigues, G.E., Johnston, P.S., Pepe, M.D., Tucker, B.S., Ramsey, M.L., Austin, L.S., 2012. Hemiarthroplasty versus reverse total shoulder arthroplasty for acute proximal humerus fractures in elderly patients. Orthopedics 35, e703–e708. https://doi.org/10.3928/01477447-20120426-25.
Gerber, C., Pennington, S.D., Nyffeler, R.W., 2009. Reverse total shoulder arthroplasty. J. Am. Acad. Orthop. Surg. 17, 284–295.
Goodman, S., Aspenberg, P., 1992. Effect of amplitude of micromotion on bone ingrowth into titanium chambers implanted in the rabbit tibia. Biomaterials 13, 944–948. https://doi.org/10.1016/0142-9612(92)90118-8.
Guery, J., Favard, L., Sirveaux, F., Oudet, D., Mole, D., Walch, G., 2006. Reverse total shoulder arthroplasty: survivorship analysis of eighty replacements followed for five to ten years. JBJS 88, 1742–1747.
Gutiérrez, S., Greiwe, R.M., Frankle, M.A., Siegal, S., Lee, W.E., 2007. Biomechanical comparison of component position and hardware failure in the reverse shoulder prosthesis. J. Shoulder Elbow Surg. 16, S9–S12.
Harman, M., Frankle, M., Vasey, M., Banks, S., 2005. Initial glenoid component fixation in "reverse" total shoulder arthroplasty: a biomechanical evaluation. J. Shoulder Elbow Surg. 14, 162S–167S. https://doi.org/10.1016/j.jse.2004.09.030.
Hattrup, S.J., 2010. The influence of postoperative acromial and scapular spine fractures on the results of reverse shoulder arthroplasty. Orthopedics 33, 302. https://doi.org/10.3928/01477447-20100329-04.
Hoenig, M.P., Loeffler, B., Brown, S., Peindl, R., Fleischli, J., Connor, P., D'Alessandro, D., 2010. Reverse glenoid component fixation: is a posterior screw necessary? J. Shoulder Elbow Surg. 19, 544–549.
Humphrey, C.S., Kelly, J.D., Norris, T.R., 2008. Optimizing glenosphere position and fixation in reverse shoulder arthroplasty, Part Two: the three-column concept. J. Shoulder Elbow Surg. 17, 595–601. https://doi.org/10.1016/j.jse.2008.05.038.
Irlenbusch, U., Kohut, G., 2015. Evaluation of a new baseplate in reverse total shoulder arthroplasty – comparison of biomechanical testing of stability with roentgenological follow up criteria. Orthop. Traumatol. Surg. Res. 101, 185–190. https://doi.org/10.1016/j.otsr.2014.11.015.
James, J., Allison, M.A., Werner, F.W., McBride, D.E., Basu, N.N., Sutton, L.G., Nanavati, V.N., 2013. Reverse shoulder arthroplasty glenoid fixation: is there a benefit in using four instead of two screws? J. Shoulder Elbow Surg. 22, 1030–1036.
Jasty, M., Bragdon, C., Burke, D., O'Connor, D., Lowenstein, J., Harris, W.H., 1997. In vivo skeletal responses to porous-surfaced implants subjected to small induced motions. J. Bone Joint Surg. Am. 79, 707–714.
Klein, S.M., Dunning, P., Mulieri, P., Pupello, D., Downes, K., Frankle, M.A., 2010. Effects of acquired glenoid bone defects on surgical technique and clinical outcomes in reverse shoulder arthroplasty. J. Bone Joint Surg. Am. 92, 1144–1154. https://doi.org/10.2106/JBJS.I.00778.
Königshausen, M., Jettkant, B., Sverdlova, N., Ehlert, C., Gessmann, J., Schildhauer, T. A., Seybold, D., 2015. Influence of different peg length in glenoid bone loss: a biomechanical analysis regarding primary stability of the glenoid baseplate in reverse shoulder arthroplasty. Technol. Health Care 23, 855–869.
Lenarz, C., Shishani, Y., McCrum, C., Nowinski, R.J., Edwards, T.B., Gobezie, R., 2011. Is reverse shoulder arthroplasty appropriate for the treatment of fractures in the older patient? Early observations. Clin. Orthop. 469, 3324–3331. https://doi.org/10.1007/s11999-011-2055-z.
Martin, E.J., Duquin, T.R., Ehrensberger, M.T., 2017. Reverse total shoulder glenoid baseplate stability with superior glenoid bone loss. J. Shoulder Elbow Surg. 26, 1748–1755.
Nikooyan, A.A., Veeger, H.E.J., Westerhoff, P., Graichen, F., Bergmann, G., van der Helm, F.C.T., 2010. Validation of the Delft Shoulder and Elbow Model using in-vivo glenohumeral joint contact forces. J. Biomech. 43, 3007–3014. https://doi.org/10.1016/j.jbiomech.2010.06.015.
Nyffeler, R.W., Werner, C.M., Gerber, C., 2005. Biomechanical relevance of glenoid component positioning in the reverse Delta III total shoulder prosthesis. J. Shoulder Elbow Surg. 14, 524–528.
Otto, R.J., Virani, N.A., Levy, J.C., Nigro, P.T., Cuff, D.J., Frankle, M.A., 2013. Scapular fractures after reverse shoulder arthroplasty: evaluation of risk factors and the reliability of a proposed classification. J. Shoulder Elbow Surg. 22, 1514–1521. https://doi.org/10.1016/j.jse.2013.02.007.
Parsons, B.O., Gruson, K.I., Accousti, K.J., Klug, R.A., Flatow, E.L., 2009. Optimal rotation and screw positioning for initial glenosphere baseplate fixation in reverse shoulder arthroplasty. J. Shoulder Elbow Surg. 18, 886–891.
Pilliar, R.M., Lee, J.M., Maniatopoulos, C., 1986. Observations on the effect of movement on bone ingrowth into porous-surfaced implants. Clin. Orthop., 108–113
Roche, C.P., Stroud, N.J., Martin, B.L., Steiler, C.A., Flurin, P.-H., Wright, T.W., DiPaola, M.J., Zuckerman, J.D., 2013a. The impact of scapular notching on reverse shoulder glenoid fixation. J. Shoulder Elbow Surg. 22, 963–970. https://doi.org/10.1016/j.jse.2012.10.035.
Roche, C.P., Stroud, N.J., Martin, B.L., Steiler, C.A., Flurin, P.-H., Wright, T.W., Zuckerman, J.D., DiPaola, M.J., 2013b. Achieving fixation in glenoids with superior wear using reverse shoulder arthroplasty. J. Shoulder Elbow Surg. 22, 1695–1701. https://doi.org/10.1016/j.jse.2013.03.008.
Sirveaux, F., Favard, L., Oudet, D., Huquet, D., Walch, G., Molé, D., 2004. Grammont inverted total shoulder arthroplasty in the treatment of glenohumeral osteoarthritis with massive rupture of the cuff. Results of a multicentre study of 80 shoulders. J. Bone Joint Surg. Br. 86, 388–395.
Stechel, A., Fuhrmann, U., Irlenbusch, L., Rott, O., Irlenbusch, U., 2010. Reversed shoulder arthroplasty in cuff tear arthritis, fracture sequelae, and revision arthroplasty. Acta Orthop. 81, 367–372. https://doi.org/10.3109/17453674.2010.487242.
Stephens, B.F., Hebert, C.T., Azar, F.M., Mihalko, W.M., Throckmorton, T.W., 2015. Optimal baseplate rotational alignment for locking-screw fixation in reverse total shoulder arthroplasty: a three-dimensional computer-aided design study. J. Shoulder Elbow Surg. 24, 1367–1371. https://doi.org/10.1016/j.jse.2015.01.012.
Stroud, N.J., DiPaola, M.J., Martin, B.L., Steiler, C.A., Flurin, P.-H., Wright, T.W., Zuckerman, J.D., Roche, C.P., 2013. Initial glenoid fixation using two different reverse shoulder designs with an equivalent center of rotation in a low-density and high-density bone substitute. J. Shoulder Elbow Surg. 22, 1573–1579. https://doi.org/10.1016/j.jse.2013.01.037.
TA Instruments, 2015. ElectroForce 3330 Series II Test Instrument Data Sheet; http://www.tainstruments.com/wp-content/uploads/brochure_3330_SeriesII.pdf.
Wall, B., Nové-Josserand, L., O'Connor, D.P., Edwards, T.B., Walch, G., 2007. Reverse total shoulder arthroplasty: a review of results according to etiology. J. Bone Joint Surg. Am. 89, 1476–1485. https://doi.org/10.2106/JBJS.F.00666.
Werner, C.M.L., Steinmann, P.A., Gilbart, M., Gerber, C., 2005. Treatment of painful pseudoparesis due to irreparable rotator cuff dysfunction with the Delta III reverse-ball-and-socket total shoulder prosthesis. J. Bone Joint Surg. Am. 87, 1476–1486. https://doi.org/10.2106/JBJS.D.02342.
Westerhoff, P., Graichen, F., Bender, A., Halder, A., Beier, A., Rohlmann, A., Bergmann, G., 2009. In vivo measurement of shoulder joint loads during activities of daily living. J. Biomech. 42, 1840–1849. https://doi.org/10.1016/j.jbiomech.2009.05.035.
Winter, D.A., 1990. Biomechanics and Motor Control of Human Movement. Wiley-Interscience Publication, New York.
Yang, C.-C., Lu, C.-L., Wu, C.-H., Wu, J.-J., Huang, T.-L., Chen, R., Yeh, M.-K., 2013. Stress analysis of glenoid component in design of reverse shoulder prosthesis using finite element method. J. Shoulder Elbow Surg. 22, 932–939.
Zumstein, M.A., Pinedo, M., Old, J., Boileau, P., 2011. Problems, complications, reoperations, and revisions in reverse total shoulder arthroplasty: a systematic review. J. Shoulder Elbow Surg. 20, 146–157. https://doi.org/10.1016/j.jse.2010.08.001.